Revision 2

Discovery of terrestrial andreyivanovite, FeCrP, and the effect of Cr and V substitution in barringerite-allabogdanite low-pressure transition.

Word counts: 6115

Evgeny V. Galuskin[1*], Joachim Kusz[2], Irina O. Galuskina[1], Maria Książek[2], Yevgeny Vapnik[3], Grzegorz Zieliński[4]

[1]Faculty of Natural Sciences, University of Silesia, Będzińska 60, 41-200 Sosnowiec, Poland;

[2]Faculty of Science and Technology, University of Silesia, ul. 75. Pułku Piechoty 1, 41-500 Chorzów, Poland;

[3]Department of Geological and Environmental Sciences, Ben-Gurion University of the Negev, P.O.B. 653, Beer-Sheva 84105, Israel; vapnik@bgu.ac.il;

[4]Micro-Area Analysis Laboratory, Polish Geological Institute—National Research Institute, Rakowiecka 4, 00-975 Warsaw, Poland; gzie@pgi.gov.pl.

*e-mail: evgeny.galuskin@us.edu.pl; ORCID 0000-0002-7018-527X

Abstract

Iron phosphides with significant variations of Cr (up to 18 wt.%) and V (up to 8.6 wt.%) content were detected in gehlenite-bearing breccia at the Hatrurim Complex, Negev desert, Israel. Investigations of composition and structure of the Fe_2P phosphides showed that when V+Cr content is higher than 0.26 apfu (atom per formula unite), a transition from the hexagonal

barringerite (*P*-62*m*) to orthorhombic allabogdanite (*Pnma*) takes place. According to the experimental data, allabogdanite is a high-pressure (>8GP) polymorph of barringerite. Pseudowollastonite associated with Cr-V-bearing allabogdanite is an indicator of phosphide crystallization at a high temperature (>1200°C) and low pressure. Thus, at the low pressure close to ambient, when more than 13 at.% Fe in Fe_2P is substituted by Cr and V, the orthorhombic polymorph is stable. The orthorhombic phosphide with the highest Cr and V contents belongs to andreyivanovite species with the FeCrP end-member formula. This is the first finding on Earth of that very rare mineral described from the Kaidun meteorite. Some Cr-V-bearing phosphides have an unusual morphology, which cannot be explained by crystallization from a melt. More probably, these phosphides can form in the process of replacing fish bone remains. We believe that sedimentary protolith was not thermally altered and contained a significant amount of bituminous organic matter and phosphorite inclusions. Injecting paralava into the sedimentary rocks determines the conditions for phosphide formation on the boundary of these rocks as a result of the high-temperature carbothermal reduction process.

Keywords: terrestrial natural phosphides, barringerite, allabogdanite, andreyivanovite, phase transition, Hatrurim Complex

Statements and Declarations

The authors declare no conflicts of interest.

The authors declare no financial interests that are directly or indirectly related to the work submitted for publication.

Introduction

A vanadium-bearing andreyivanovite, FeCrP, in association with Cr-V-bearing Fe_2P polymorphs – barringerite and allobogdanite, was found in pseudowollastonite-bearing gehlenite paralava of the Hatrurim Complex, Negev Desert, Israel. Andreyivanovite is a rare mineral, which was discovered in the Kaidun meteorite (Zolensky et al. 2008) and later was noted in Rumuruti chondrite (Greshake 2014).

The Hatrurim Complex has recently become known as a source of terrestrial phosphides (Britvin et al. 2015). Here, besides the phosphides typical of meteorites: schreibersite, Fe_3P (Britvin et al. 2021a), barringerite, Fe_2P (Britvin et al. 2017) and its high-pressure analog – allobogdanite (Britvin et al. 2021b), nine new phosphides: halamishite, Ni_5P_4 (Britvin et al. 2020a); negevite, NiP_2 (Britvin et al. 2020b); nazarovite, $Ni_{12}P_5$ (Britvin et al. 2022a); zuktamrurite, FeP_2 (Britvin et al. 2019a); transjoardanite, Ni_2P (Britvin et al. 2020c); polekhovskyite, $MoNiP_2$ (Britvin et al. 2022b); murashkoite, FeP (Britvin et al. 2019b); nickolayite, FeMoP (Murashko et al. 2019); orishchinite, Ni_2P (Britvin et al. 2019c) were discovered. This detection of phosphides in the rocks of the Hatrurim Complex is unexpected. This is true both for the Hatrurim Complex, whose mineral association mainly formed in oxidizing conditions (Galuskina et al. 2017), and for the rocks of the terrestrial genesis on the whole. Phosphides were detected in samples of diopside paralava collected in a small quarry in the Daba Siwaqa pyrometamorphic rock field in Jordan (Britvin et al. 2015) and in the two rock samples found *ex situ* in dry wadies Halamish (diopside paralava) and Zohar (gehlenite paralava), the Hatrurim Basin, Negev Desert, Israel (Britvin et al. 2015; Galuskin et al. 2020). In 2019, we found a bedrock of gehlenite paralava in the Zohar wadi, the study of which led to the discovery of V-bearing andreyivanovite and Cr-V-bearing allabogdanite, aggregations of which resemble fossilized organic fragments.

This is the peer-reviewed, final accepted version for American Mineralogist, published by the Mineralogical Society of America.
The published version is subject to change. Cite as Authors (Year) Title. American Mineralogist, in press.
DOI: https://doi.org/10.2138/am-2022-8647. http://www.minsocam.org/

Allabogdanite is a high-pressure polymorph of barringerite. A synthetic orthorhombic Fe_2P is stable at the pressure limit 8-40 GPa and a temperature about 1100°C (Dera et al. 2008). Natural barringerite with low Ni (up to 0.1 apfu) and Mo (up to 0.04 apfu) impurities transfers to allobogdanite at 25 ± 3 GPa and at a temperature 1400 ± 100°C (Britvin et al. 2021b). On the other hand, Litasov et al. (2020) concluded on the basis of theoretical calculations and experimental data that allabogdanite is a lower-temperature phase compared to barringerite, which is stable at the ambient pressure and temperature lower than 500°C. Unlike isostructural high pressure and high-temperature allabogdanite, a synthetic analog of andreyivanovite crystallizes from a high-temperature melt at ambient pressure (Kumar et al. 2004).

In this paper, we present the results of an investigation of the morphology, composition and structure of the natural Fe_2P-based phosphides with wide variations of Cr (up to 18.5 wt.%) and V (up to 8 wt.%) contents from pyrometamorphic rocks of the Hatrurim Complex. For the first time, we describe andreyivanovite from the terrestrial rocks, discuss the possibility of Cr-V-bearing phosphide formation after fish bone remains and conditions of allabogdanite crystallization at a low pressure. The boundaries of the mineral species barringerite, allabogdanite and andreyivanovite in the Fe_2P – FeCrP (+FeVP) series are considered in the paper.

Samples and methods of investigation

More than 300 samples of phosphide-bearing breccia were collected during field trips in 2019 and 2021, and in the two samples barringerite stoichiometry phosphides with high Cr and V contents were revealed. The morphology and chemical composition of phosphides and associated minerals were investigated using Philips XL30, Phenom XL and Quanta 250 EDS-equipped scanning electron microscopes (Institute of Earth Sciences, University of Silesia, Poland). The

This is the peer-reviewed, final accepted version for American Mineralogist, published by the Mineralogical Society of America.
The published version is subject to change. Cite as Authors (Year) Title. American Mineralogist, in press.
DOI: https://doi.org/10.2138/am-2022-8647. http://www.minsocam.org/

chemical composition of Cr-V-bearing phosphides was measured with a Cameca SX100 electron microprobe analyzer (EMPA, Micro-Area Analysis Laboratory, Polish Geological Institute—National Research Institute, Warsaw, Poland): WDS, accelerating voltage = 15 kV, beam current = 40 nA, beam diameter ~1 μm. The following standards and lines were used: apatite = Ca*K*α, P*K*α; rutile = Ti*K*α; Ni metal = Ni*K*α; Cu metal = Cu*K*α; hematite = Fe*K*α; V metal = V*K*α; Cr_2O_3 = Cr*K*α. Mg, Si, Al, S, Mn, Se, Co, As, Mo, Sb are lower detection limits.

Single-crystal X-ray studies of phosphide crystals were carried out using a SuperNova diffractometer with a mirror monochromator (MoKα, λ = 0.71073 Å) and an Atlas CCD detector (Agilent Technologies) at the Institute of Physics, University of Silesia, Poland. The structures of Fe_2P (Carlsson et al. 1973) and FeCrP (Kumar et al. 2004) were taken as the initial model. Subsequently, the phosphide structures were refined using the SHELX97 program (Sheldrick 2015).

The bulk chemical composition of breccia was investigated with an ICP-MS (inductively coupled plasma mass spectrometry), and analyses were performed in the ACME Laboratory in Vancouver, BC, Canada.

Geological setting, short description of rocks, morphology and phosphides composition

Pyrometamorphic rocks of the Hatrurim Complex (Molted Zone) is mainly represented by spurrite marbles, larnite pseudoconglomerates, gehlenite hornfelses and paralavas of different composition formed in sanidinite facies conditions (Bentor et al. 1963; Gross 1977; Burg et al. 1991, 1999; Vapnik et al. 2007; Novikov et al. 2013; Galuskina et al. 2014). The products of low-temperature alteration of pyrometamorphic rocks also belong to the Hatrurim Complex. The Complex forms outcrops in areas up to a few hundred square kilometers, stretching along the

Dead Sea Rift in the territories of Israel, Jordan and Palestine (Novikov et al. 2013). So far the genesis of the Hatrurim Complex rocks has been an issue of some debate. The early hypothesis assumed that the pyrometamorphic alteration of these rocks took place at the expense of burning bitumen contained in sedimentary protolith (Burg et al. 1991, 1999). The recently proposed "mud volcano" hypothesis suggests that the burning of a sedimentary protolith represented mainly by Maastrichtian bituminous rocks (Ghareb Formation in Israel, Burg et al. 1991) was fueled by methane from gas traps located in the tectonically active Dead Sea Rift zone (Sokol et al. 2010; Novikov et al. 2013). One of the pieces evidence of a gas participant in the process of pyrometamorphic rock formation in the Hatrurim Complex is the presence within them of explosive channels, explosive breccias and clastic dikes filled by fragments cemented by later low-temperature minerals (Sokol et al. 2007, 2010).

Phosphide-bearing rocks were found in an outcrop in a man-made exposure situated in the biggest area of pyrometamorphic rocks of the Hatrurim Complex in Israel, known as the Hatrurim Basin (Gross 1977). The outcrop formed as a result of the Arad-Dead Sea road building is 5 km out of the Hatrurim crossroads to the north-east in the Negev Desert (Fig. 1A). A large part of the outcrop comprises coarse-layered low-temperature calcite-hydrosilicate-hydrogrossular rocks forming after pyrometamorphic rocks. In the north part of the outcrop, brecciated fragments of grey, pink, brown hydrogrossular rock cemented by dark gehelenite paralava were observed (Fig. 1A-C). On the boundary of hydrogrossular rock and paralava, zonal oval aggregates of minerals of the Fe-P(±C) system reach 1-1.5 cm in size (Figs. 1D, 2A) The following mineral sequence is observed in these aggregates from core to rim: barringerite, schreibersite and schreibersite-iron (±cohenite) eutectic (Figs. 1D, 2B). In the near-contact zone of paralava, xenomorphic aggregates of schreibersite-iron (±cohenite) eutectic and iron with

schreibersite peritectic were found (Fig. 2C, D). Barringerite is replaced by porous aggregates of murashkoite, FeP. Pyrrhotite often overgrows on minerals of the Fe-P(±C) system (Fig. 2B).

Paralava is inhomogeneous and exhibits a flow texture underlined by gas bubbles filled by calcite, tacharanite, ettringite and gypsum. Weakly altered black fragments of paralava from the central part of big rock blocks are represented by gehlenite-flamite/larnite (polymorphs of Ca_2SiO_4) rock enriched in pyrrhotite (Fig. 2E). Some parts of the paralava, in which flamite is almost completely replaced by rankinite, $Ca_3Si_2O_7$, are observed. At the contact of hydrogrossular rock, flamite and rankinite are replaced by pseudowollastonite, $Ca_3(Si_3O_9)$ (Fig. 2A), and more rarely by cuspidine, $Ca_4(Si_2O_7)F_2$. Accessory minerals of paralava are presented by fluorapatite, Si-Cr-bearing perovskite, magnesiochromite, more rarely by schreibersite, native iron, schreibersite-iron eutectic and wüstite. Very rare phosphides contain graphite inclusions and are intergrown with osbornite, TiN (see Fig. 3F). Primary minerals of paralava are replaced by hydrogrossular, tacharanite, tobermorite and calcite.

Hydrogrossular rock cemented by paralava has a sponge, porous structure, whose space is partially filled by tacharanite and calcite (Fig. 2F). The rock is colored pink and red by iron oxides. In hydrogrossular rock, small relics of barringerite, murashkoite, perovskite, pseudowollastonite and cuspidine are noted (Fig. 2F).

A comparison of the geochemical data obtained for gehlenite paralava and hydrogrossular rock displays that these rocks have probably the same sedimentary protolith, whose composition differs sharply from the bitumen chalk of the Ghareb Formation (Table S1; Fig. S1).

Iron phosphides in pyrometamorphic rocks usually have low concentrations of Ni, Cr, V and Ti impurities, up to 2-3 wt.% (Britvin et al. 2017; 2021). Phosphides with high Cr and V contents were revealed inside a light pseudowollastonite paralava tongue in hydrogrossular rock (Figs. 3A, 4A). Pseudowollastonite paralava with gehlenite relics contains fragments enriched in

cuspidine and perovskite. Phosphides form indiscrete grain groups, single xenomorphic grains and very rare well-formed flattened crystals (Fig. 3D-E). In several cases, phosphide aggregates exhibit unusual morphology: as rings with thickening, semi-rings with bulges, straight bands with changing thickness and branches, hoked forms, series of jagged grains etc. (Fig. 4B-D). These phosphide aggregates consist of relatively large and homogeneous mono-crystalline fragments 10-40 μm in size (Fig. S2).

More than 250 analyses of phosphides from the pseudowollastonite paralava tongues shown in Figs. 3A, 4A using an EDS detector were obtained. Points of these hit the narrow elongated field in Fe_2P-FeCrP-FeVP diagram (Fig. 5). Five groups of grains were distinguished, whose composition was established using a microprobe analyzer (Table 1). From every group, crystals 10-40 μm in size were selected for structural investigation, totaling 41 crystals. All crystals were tested on a single-crystal XRD (SCXRD) diffractometer and the diffraction data were collected for the best-quality grains in every group (Table 2, Supplementary materials: CIF files and Tables S2-4).

Phosphide structure, influence of Cr and V impurities on phase transition barringerite → allabogdanite, mineral species boundaries

Phosphide crystals from group number 1 (1a and 1b subgroup) with low Cr and V contents (Cr+V < 0.1 apfu, Table 1) have a hexagonal structure of the barringerite type (Table 2). The results obtained for the 2 crystal group with a Cr+V content of about 0.26 apfu are interesting (Table 1). One of the crystals from this group has a hexagonal structure and the next two crystals show the orthorhombic symmetry and the structure of the allabogdanite type (Table 2). All the crystals from the 3-5 groups with a Cr+V higher than 0.35 apfu (Table 1) have an

orthorhombic structure of the allabogdanite type (Table 2). The hexagonal structure of barringerite and orthorhombic structure of allabogdanite/andreyivanovite are similar. The layers with a hexagonal motive are distinguished in both structure types (Fig. S3). In barringerite there are two different intercalated layers, one of which is represented by connected vertices tetrahedra centered by Fe coordinated by P (Fig. S3A). The second layer is formed by laying tetragonal Fe-pyramids on their side, which are interconnected both edges and vertices (Fig. S3B). Cr and V only substitute for Fe at pyramidal sites. As Cr and V have slightly bigger metallic radii than Fe, they influence the increase in the ***c*** parameter of barringerite when the Cr+V content rises (Table 2, Fig. 6). In the orthorhombic phosphides with an allabogdanite structure, the ***b*** parameter corresponds to the ***c*** parameter in barringerite (Table 2). The ***b*** parameter of allabogdanite is ~0.08Å more than the ***c*** parameter of barringerite of the close composition (Fig. 6). The parameter ***b*** in orthorhombic phosphides does not depend on the content of Cr and V (Table 2, Fig. 6). An increase in the Cr+V content is accompanied by an enlargement of the distance between the metal and apical phosphorus in a tetragonal pyramid in the plane perpendicular to ***b*** (Fig. 6, Table S4).

In the Fe_2P-FeCrP-FeVP ternary diagram (Fig. 5), the points of the 1-3 groups from the phosphide analyses placed at the Fe_2P field, the points of the 4 group phosphide analyses are near the boundary Fe_2P-FeCrP, and the points of the 5 groups from the phosphide analyses touch the andreyivanovite field. The structural data obtained for the 2 groups of phosphides allow us to conclude that allabogdanite is stable when Cr+V content is more than 0.26 apfu (Fig. 6). The mineral species boundary between barringerite and allabogdanite in the Fe_2P-FeCrP-FeVP classification diagram runs to approximately 0.26 Cr+V pfu (Fig. 5). The phase transition *P*-62*m* (barringerite) → *Pnma* (allabogdanite) is observed for the composition close to the

$Fe_{1.74}(Cr,V)_{0.26}P$, i.e. substitution more than 13 at. % of Fe in Fe_2P by Cr+V leads to the stabilization of the orthorhombic structure of allabogdanite. Phosphides from the paralava studied are formed in conditions of high temperature and low pressure, and this fact is confirmed by the results of mineral paragenetic analysis, as presented below.

Discussion

The Hatrurim Complex is the only known terrestrial source of large phosphide aggregates (Fig. 1D; Britvin et al. 2015). All known finds of barringerite and shreibersite in the terrestrial rock are reported as a rare occurrence, often with unclear or exotic origin: iron-bearing sediment-contaminated andesitic and dacitic lavas, fulgurites, natural and anthropogenic burned coal-bearing rocks and others (Pedersen 1981; Borodaev 1982; Kegiao et al. 1983; Yang et al. 2005; Drake et al. 2018; Nishinbaev et al. 2002; Astakhova et al. 2014; Plyashkevich et al. 2016; Savina et al. 2020; Bunch et al. 2021).

The formation of phosphides in rocks of the Hatrurim Complex with known geological settings (Zohar, Israel and Daba-Siwaqa, Jordan) was connected with the unique character of geological conditions during their crystallization. It is important to emphasize that within the Hatrurim Complex rock fields, there are no magmatic rocks, and the formation of pyrometamorphic rocks was caused by natural fire driven by in-going gases and organic fuel located in sedimentary rocks (Burg et al. 1991; Novikov et al. 2013). Based on the phosphide-bearing breccia study from Zohar, it can be assumed that close to the surface there was a local fire centrum (foci) generating a reduced gehlenite paralava and a significant volume of gases, which cause explosive breccia. It is not implausible that the activity of combustion foci keep in methane flows and, probably, hydrogen from an underlying gaseous-oil trap (Sokol et al. 2007; Novikov et al. 2013; Britvin et al. 2022b).

We believe that sedimentary rocks were not thermally altered and contained a significant amount of bituminous organic matters and phosphorite inclusions. Injecting paralava into the sedimentary rocks determines the conditions for aggregates of Fe-P(±C) mineral formations on the boundary of these rocks as a result of a high-temperature carbothermal reduction process involving the products of organic matter decomposition. The process is complex and multi-stage, but in general, it can be presented by the two main reactions of Fe and P reduction, respectively: $Fe_2O_3 + 3C \rightarrow 2Fe + 3CO(g)$ и $4Ca_5(PO_4)_3F + 21SiO_2 + 20Al_2O_3 + 10C \rightarrow 6P_2(g) + 10CO(g) + 20Ca_2Al_2SiO_7 + SiF_4(g)$. Partial melting of sedimentary rock clasts and contamination of this melt by paralava manifested itself in the formation of drops of molten iron on the boundary of paralava and sedimentary rocks (Figs. 1D, 2A, S4), as well as in the replacement of flamite and rankinite by pseudowollastonite and cuspidine in the near-contact part of the paralava (Fig. 2A, 4A). The process of high-temperature roast (clinkerization) of sedimentary rock debris led to the short-term generation of reducing gases as a result of the decomposition of bitumen and phosphorus-bearing fossil remains, which react with iron drops inducing a phosphides formation (Fig. 1D). Later, clinker-like rock was altered to hydrogrossular rock as a consequence of low-temperature processes (Fig. 2C). Geochemical data indicate that gehlenite paralava and hydrogrossular rock rather have the same sedimentary protolith (Table S1; Fig. S1).

The rarity of phosphides in the rocks from the Hatrurim Complex is related to the fact that the necessary condition for their formation is the injection of sulphide-bearing reduced paralava to an unaltered sedimentary rock containing organic matter and phosphorite inclusions. We observed a large number of various oxidized paralavas (diopside-bearing, rankinite-schorlomite, wollastonite, gehlenite, etc.), which were formed almost simultaneously with high-temperature host rocks in the Hatrurim complex, usually represented by gehlenite hornfelses. It is probable

that the reduced paralava with phosphides traces the channels through which combustible gases came from the underlying horizon, activating mass combustions of sedimentary organic fuel and determining the formation of large areas of pyrometamorphic rocks, as is assumed in "the mud volcano" hypothesis (Sokol et al. 2012; Novikov et al. 2013).

Sedimentary protolith is very likely to contain fragments of rocks similar in composition to phosphorites, called the P-Si-Fe and P-Si-C series, with carbonate-argillaceous cement, which is noted as separate small fields on the unconformable boundaries between the Mishash (Campanian) and Ghareb (Maastrichtian, the major protolith unit of the Hatrurim Complex) formations (Shahar et al. 1989).

Gehlenite paralava and the related phosphide mineralization of the Zohar wadi belong to the high-temperature formations of the Hatrurim Complex, which is confirmed by the following observation. Pseudowollastonite (polytype 4*M*; a = 6.8382(2)Å, b = 22.8692(3)Å, c = 19.6208(5)Å, β = 90.656(2)°, our SCXRD data) indicates the high temperature of crystallization, higher than 1200°C, and low pressure (close to ambient pressure) excluding the appearance of "clear" allabogdanite (Swamy and Dubrovinsky 1997; Dera et al. 2008; Seryotkin et al. 2012; Britvin et al. 2021b). Numerous aggregates of barringerite found on the boundary of paralava and hydrogrossular rock indicate temperature crystallization higher than 1350°C, as was established for Mongolian paralavas (Savina et al. 2020). The formation of ideal iron balls in gehlenite rock (Fig. S3B, C) is possible only at full iron melting, and can point to the temperature of paralava being higher than 1500°C locally (Persikov et al. 2019). Additionally, in phosphide-bearing paralava found *ex situ* in the lower course of the Zohar wadi, we described before repeated melting of gehlenite and flamite (Galuskin et al. 2020), which could take place at a temperature of 1400-1500°C (Mao et al. 2006).

This is the peer-reviewed, final accepted version for American Mineralogist, published by the Mineralogical Society of America.
The published version is subject to change. Cite as Authors (Year) Title. American Mineralogist, in press.
DOI: https://doi.org/10.2138/am-2022-8647. http://www.minsocam.org/

Phosphides with high Cr and V contents, which are detected within the thin tongue of pseudowollastonite paralava, form unusual and various forms. This forms is difficult to explain by melt crystallization (Fig. 4). These forms are reminiscent of fish bones, which are widely distributed in the Negev desert phosphorites underlying the rocks of the Hatrurim Complex (Fig. S5). A mechanism of phosphide formation after fishbone remains is unclear. Small paralava tongues are often angular in cross-section (Fig. 4A), which may indicate that paralava enriched in Cr (+V?) selectively intruded into the most permeable rock fragments, possibly containing numerous fish bone remains presented by CO_3-F-bearing hydroxylapatite ("francolite" with V impurity) and organic substance. Fig. 4A shows that on the boundary of pseudowollastonite paralava forming the tongue in hydrogrossular rock there is an absence of rounded mineral aggregates of the Fe-P(±C) system characteristic for contacts with gehlenite paralava (Figs. 1D, 2A). It is believed that on the boundary of pseudowollastonite paralava and sedimentary rock, processes of P and Fe reduction and phosphide formation after fishbone remains took place simultaneously. Thereafter phosphides were assimilated by paralava (Fig. 4). Schematically, the mechanism of phosphide formation is shown in Fig. S6. The process of phosphide formation was conducted in a kinetic regime, so the width of the reaction zone fluctuated and replacement of separated bone remains could be practically per saltum. In this case, assimilation of bone remains by paralava, reducing reactions involving products of organic substance decomposition and phosphide formation can be considered as one process. The possibility of phosphide formation after organic remains was previously referred to by Borodaev et al. (1982), who described a schreibersite formation in a graphitized wood elevated from a depth of 1400 m in the Red Sea.

The appearance of high concentrations of Cr and V in phosphides is associated not only with the high formation temperature and chemical heterogeneity of the protolith, but also with

very low oxygen activity. The existence of metallic Cr and V in the mineral-forming system corresponds to highly reduced conditions $fO2 < \Delta IW \sim -5$, which will facilitate the replacement of Fe in phosphides by V and Cr (Griffin et al. 2019). The appearance of osbornite in association with phosphides (Fig. 3F) is an indicator that locally the oxygen activity fell below $fO2 < \Delta IW$ -6 – -9 and met super-reduction conditions (Griffin et al. 2019). The formation of Cr-V-bearing phosphides could take place at temperatures lower than the crystallization temperature of barringerite from the melt at 1350°C.

Conclusion

Injection of paralava into the sedimentary rocks, which were not thermally altered and contained a significant amount of bituminous organic matters and phosphorite inclusions, creates the conditions for Fe-P(±C) mineral system formation on the boundary of these rocks as a result of the high-temperature carbothermal reduction process.

The morphology of the part of Cr-V-bearing phosphides aggregates resembles a form of fish bone remains in phosphorites. The replacement of fish bone remains by Cr-V-bearing phosphides at high temperatures with the preservation of their morphology can be explained by the specific reaction mechanism and the high rate of such pseudomorphs' formation.

Orthorhombic allabogdanite, Fe_2P, is formed in the stability field of hexagonal barringerite at a low pressure and a high temperature when its structure is stabilized by Cr and V impurities, which replace more than 13 at.% Fe in its structure.

The points of chemical analysis of orthorhombic phosphides with the highest contents of Cr and V from paralava of the Hatrurim Complex hit into the field of andreyivanovite, FeCrP (Fig. 5). This is the first discovery of andreyivanovite in terrestrial rocks.

Implication

For the first time, allabogdanite of the terrestrial origin was found in a sample of diopside-bearing paralava of the pyrometamorphic Hatrurim Complex from the wadi Halamish in the Negev Desert, Israel. It was supposed that allabogdanite formed after barringerite as a result of the phase transition at the very high temperature and pressure caused by meteorite impact (Britvin et al. 2021). This assumption was based on the experimental data (Dera et al. 2008). Cr-V-bearing allabogdanite, that was studied by us, has been found in pseudowollastonite-gehlenite paralava in the wadi Zohar located about 2 km from the place of the first finding of allabogdanite, and undoubtedly, formed at the low pressure. The trends of phase transition in meteorite, paralava and in experiment are shown in the phase barringerite-allabogdanite diagram (Fig. 7). The barringerite → allabogdanite phase transition has been studied only in high-temperature experiments (Dera et al. 2008; Britvin et al. 2021). In the natural systems at a relatively low temperature, this process probably proceeds very slowly and depends on a real composition of phosphide and the rate of system cooling. Rather than looking for an exotic reason of terrestrial allabogdanite origin, which would be in line with conditions of the high-temperature experiment (Fig. 7, trends 1, 4; Britvin et al. 2021), it firstly is necessary to consider the possibility of the phase transition barringerite → allabogdanite as a result of the temperature decreasing at the ambient pressure (Fig. 7, trend 5). We following Litasov et al. (2020) in believing that meteoritic allabogdanite is not a suitable reference for the terrestrial occurrences in the Hartritum complex. Allabogdanite can either form as a primary mineral at the high pressure from high-temperature melt (Fig. 7, trend 2) or as a result of the phase transition barringerite → allabogdanite at decreasing temperature (Fig. 7, trend 3). Polysynthetic twinning, which was observed in

allabogdanite from the intergrowths with barringerite from wadi Halamish (Britvin et al. 2021), probably is a criterium of the phase transition barringerite → allabogdanite. Barringerite is a metastable phase at ambient conditions, its predominance over allabogdanite both in meteorites, and in terrestrial rocks, is related to a very slow rate of the phase transition barringerite → allabogdanite at the low temperature. Cr-V-bearing allabogdanite from gehlenite-pseudowollastonite parava of wadi Zohar formed in the field of barringerite stability and its structure was stabilized by Cr and V impurities, and allabogdanite from the wadi Halamish paralava formed as a result of the phase transition barringerite → allabogdanite at the moderate temperature (<500°C). Extended heating was sustained by the combustion processes determining a formation of huge areas of pyrometamorphic rocks of the Hatrurim Complex.

Suplementarny Information

The online version contains supplementary material available at...

Acknowledgments

The investigations were partially supported by the National Science Centre (NCN) of Poland, grant no. 2021/41/B/ST10/00130.

References

Astakhova, N.V., Kolesnik, O.V. and S'edin, V.T. (2014) Ore Mineralization in Volcanic Rocks from the Submarine Rises of the Sea of Japan. Geochemistry International, 52(2), 143–160.

Bentor, Y.K., Gross, S. and Heller L. (1963) Some unusual minerals from the "Mottled Zone" complex, Israel. American Mineralogist, 48, 924–930.

Borodaev, Y.S., Bogdanov, Y.A. and Vyalsov, L.N. (1982) New nickel-free variety of schreibersite Fe_3P. Proceedings of the All-Union Mineralogical Society, 111(6), 682–687 (in Russian).

Britvin, S.N., Murashko, M.N., Vapnik, Ye., Polekhovsky, Y.S. and Krivovichev, S.V. (2015) Earth's phosphides in Levant and insights into the source of Archean prebiotic phosphorus. Scientific Reports, 5, 8355.

Britvin, S.N., Murashko, M.N., Vapnik, E., Polekhovsky, Y.S. and Krivovichev, S.V. (2017) Barringerite Fe_2P from pyrometamorphic rocks of the Hatrurim Formation, Israel. Geology of Ore Deposits, 59, 619–625.

Britvin, S.N., Murashko, M.N., Vapnik, Ye., Polekhovsky, Y.S., Krivovichev, S.V., Vereshchagin, O.S., Vlasenko, N.S., Shilovskikh and V.V., Zaitsev, A.N. (2019a) Zuktamrurite, FeP_2, a new mineral, the phosphide analogue of löllingite, $FeAs_2$. Physics and Chemistry of Minerals, 46, 361–369.

Britvin, S.N., Vapnik, Ye., Polekhovsky, Y.S., Krivovichev, S.V., Krzhizhanovkaya, M.G., Gorelova, L.A., Vereshchagin, O.S., Shilovskikh, V.V. and Zaitsev, A.N. (2019b) Murashkoite, FeP, a new terrestrial phosphide from pyrometamorphic rocks of the Hatrurim Formation, Southern Levant. Mineralogy and Petrology,113, 237–248.

Britvin, S.N., Murashko, M.N., Vapnik, Ye., Zaitsev, A.N., Shilovskikh, V.V., Vasiliev, E.A.,

Krzhizhanovskaya, M.G. and Vlasenko, N.S. (2019c) IMA 2019-039. CNMNC Newsletter No. 51; European Journal of Mineralogy, 31, 1099-1104.

Britvin, S.N., Shilovskikh, V.V., Pagano, R., Vlasenko, N.S., Zaitsev, A.N., Krzhizhanovskaya, M.G., Lozhkin, M.S., Zolotarev, A.A. and Gurzhiy, V.V. (2019d) Allabogdanite, the high-pressure polymorph of $(Fe,Ni)_2P$, a stishovite-grade indicator of impact processes in the Fe–Ni–P system. Scientific Reports, 9,1047.

Britvin, S.N., Murashko, M.N., Vapnik, Ye., Polekhovsky, Y.S., Krivovichev, S.V., Vereshchagin, O.S., Shilovskikh, V.V., Vlasenko, N.S. and Krzhizhanovskaya, M.G. (2020a) Halamishite, Ni_5P_4, a new terrestrial phosphide in the Ni-P system. Physics and Chemistry of Minerals, 47(1), 3-7.

Britvin, S.N., Murashko, M.N., Vapnik, Ye., Polekhovsky, Y.S., Krivovichev, S.V., Vereshchagin, O.S., Shilovskikh, V.V. and Krzhizhanovskaya, M.G. (2020b) Negevite, the pyrite-type NiP_2, a new terrestrial phosphide. American Mineralogist, 105, 422–427.

Britvin, S.N., Murashko, M.N., Vapnik, Ye., Polekhovsky, Y.S., Krivovichev, S.V., Krzhizhanovskaya, M.G., Vereshchagin, O.S., Shilovskikh, V.V. and Vlasenko, N.S. (2020c) Transjordanite, Ni_2P, a new terrestrial and meteoritic phosphide, and natural solid solutions barringerite-transjordanite (hexagonal Fe_2P-Ni_2P). American Mineralogist, 105, 428–436.

Britvin, S.N., Krzhizhanovskaya, M.G., Zolotarev, A.A., Gorelova, L.A., Obolonskaya, E.V., Vlasenko, N.S., Shilovskikh, V.V. and Murashko, M.N. (2021a) Crystal chemistry of schreibersite, $(Fe,Ni)_3P$. American Mineralogist, 106, 1520-1529.

Britvin, S.N., Vereshchagin, O.S., Shilovskikh, V.V., Krzhizhanovskaya, M.G., Gorelova, L.A., Vlasenko, N.S., Pakhomova, A.S., Zaitsev, A.N., Zolotarev, A.A., Bykov, M., Lozhkin,

M.S. and Nestola, F. (2021b) Discovery of terrestrial allabogdanite $(Fe,Ni)_2P$, and the effect of Ni and Mo substitution on the barringerite-allabogdanite high-pressure transition. American Mineralogist, 106, 944-952.

Britvin, S.N., Murashko, M.N., Krzhizhanovskaya, M.G., Vereshchagin, O.S., Vapnik, Ye., Shilovskikh, V.V., Lozhkin, M.S. and Obolonskaya, E.V. (2022a) Nazarovite, $Ni_{12}P_5$, a new terrestrial and meteoritic mineral structurally related to nickelphosphide, Ni_3P. American Mineralogist, 107, in press. https://doi.org/10.2138/am-2022-8219.

Britvin, S.N., Murashko, M.N., Vereshchagin, O.S., Vapnik, Ye., Shilovskikh, V.V., Vlasenko, N.S. and Permyakov, V.V. (2022b) Expanding the speciation of terrestrial molybdenum: discovery of polekhovskyite, $MoNiP_2$, and insights into the sources of Mo-phosphides in the Dead Sea Transform area. American Mineralogist, 107, in press. https://doi.org/10.2138/am-2022-8261.

Bunch, T.E., LeCompte, M.A., Adedeji, A.V., Wittke, J.H., Burleigh, T.D., Hermes, R.E., Mooney, C., Batchelor, D., Wolbach, W.S., Kathan, J., Kletetschka, G., Patterson, M.C.L., Swindel, E.C., Witwe,r T., Howard, G.A., Mitra, S, Moore, C.R., Langworthy, K., Kennett, J.P., West, A. and Silvia, P.J. (2021) A Tunguska sized airburst destroyed Tall el-Hammam a Middle Bronze Age city in the Jordan Valley near the Dead Sea. Scientific Reports, 11, 18632.

Burg, A., Starinsky, A., Bartov, Y. and Kolodny, Y. (1992) Geology of the Hatrurim Formation ("Mottled Zone") in the Hatrurim basin. Israel Journal of Earth Sciences, 40, 107–124.

Burg, A., Kolodny, Y. and Lyakhovsky, V. (1999) Hatrurim-2000: the "Mottled Zone" revisited, forty years later. Israel Journal of Earth Sciences, 48, 209–223

Carlsson, B., Golin, M. and Rundqvist, S. (1973) Determination of the homogenity range and refinement of the crystal structure of Fe_2P. Journal of Solid State Chemistry, 8, 57-67.

Dera, P., Lavina, B., Borkowski, L.A., Prakapenka, V.B., Sutton, S.R., Rivers, M.L., Downs, R.T., Boctor, N.Z. and Prewitt, C.T. (2008) High-pressure polymorphism of Fe_2P and its implications for meteorites and Earth's core. Geophysical Research Letters, 35, L10301.

Drake, S.M., Beard, A.D., Jones, A.P., Brown, D.J., Fortes, A.D., Millar, I.L., Carter, A., Baca, J. and Downes, H. (2018) Discovery of a meteoritic ejecta layer containing unmelted impactor fragments at the base of Paleocene lavas, Isle of Skye, Scotland. Geology, 46(2), 171-174.

Galuskin, E., Galuskina, I., Vapnik, Y. and Murashko, M. (2020) Molecular Hydrogen in Natural Mayenite. Minerals, 10(6), 560.

Galuskina, I.O., Vapnik, Y., Lazic, B., Armbruster, T., Murashko, M. and Galuskin, E.V. (2014) Harmunite $CaFe_2O_4$: A new mineral from the Jabel Harmun, West Bank, Palestinian Autonomy, Israel. American Mineralogist, 99, 965–975.

Galuskina, I.O., Galuskin, E.V., Pakhomova, A.S., Widmer, R., Armbruster, T., Krüger, B., Grew, E.S., Vapnik, Y., Dzierażanowski, P. and Murashko, M. (2017) Khesinite, $Ca_4Mg_2Fe^{3+}_{10}O_4[(Fe^{3+}_{10}Si_2)O_{36}]$, a new rhönite-group (sapphirine supergroup) mineral from the Negev Desert, Israel – natural analogue of the SFCA phase. European Journal of Mineralogy, 29(1):101–116.

Greshake, A. (2014) Strongly hydrated microclast in the Rumuruti chondrite NWA 6828: Implications for the distribution of hydrous material in the solar system. Meteoritics and Planetary Science, 49(5), 824–841.

Griffin, W.L., Gain, S.E., Huang, J.-X., Saunders, M., Shaw, J., Toledo, V. and O'Reilly, S.Y., (2019) A terrestrial magmatic hibonite-grossite-vanadium assemblage: desilication and extreme reduction in a volcanic plumbing system, Mount Carmel, Israel. American Mineralogist, 104, 207–219.

Gross, S. (1977) The mineralogy of the Hatrurim Formation, Israel. Geological Survey Israel Bulletin, 70, 1–80.

Kegiao, C., Zaimiao, J. and Zhizhong, P. (1983) The discovery of iron barringerite (Fe_2P) in China. Acta Geologica Sinica, 199-202 (in Chinese with English abstract).

Kumar, S., Krishnamurthy, A., Bipin, K., Srivastava, K., Daa, A., Paranjpe, S. (2004) Magnetization and neutron diffraction studies on FeCrP. Pramana, 63, 199–205.

Litasov, K.D., Bekker, T.B., Sagatov, N.E., Gavryushkin, P.N., Krinitsyn, P.G. and Kuper, K.E. (2020) $(Fe,Ni)_2P$ allabogdanite can be an ambient pressure phase in iron meteorites. Scientific Reports, 10, 8956.

Mao, H., Hillert, M., Selleby M. and Sundman, B. (2006) Thermodynamic assessment of the $CaO–Al_2O_3–SiO_2$ system. Journal of the American Ceramic Society, 89(1), 298-308.

Murashko, M.N., Vapnik, Y., Polekhovsky, Y.P., Shilovskikh, V.V., Zaitsev, A.M., Vereshchagin, O.S. and Britvin, S.N. (2019) Nickolayite, IMA 2018-126. CNMNC Newsletter No. 47, February 2019, page 202; Eur. J. Mineral. 31, 199–204.

Nishinbaev, T.P., Rochev, A.V. and Kotlyarov, V.A. (2002) Iron phosphides from combustion dumps of Chelaybinsk coal basin. Uralian Geological Journal, 25(1), 105-114 (in Russian).

Novikov, I., Vapnik, Y. and Safonova, I. (2013) Mud volcano origin of the Mottled Zone, South Levant. Geoscience Frontiers, 4, 597–619.

Pedersen, A.K. (1981) Armalcolite-bearing Fe–Ti oxide assemblages in graphite-equilibrated salic volcanic rocks with native iron from Disko, central West Greenland. Contributions to Mineralogy and Petrology, 77, 307–324.

Persikov, E.S., Bukhtiyarov, P.G., Aranovich L.Y., Nekrasov, A.N. and Shaposhnikov, O.Y. (2019) Experimental simulation of the process formation of native metals (Fe, Ni, Co) in

the earth's crust during the interaction of hydrogen with basalt melts. Geochemistry, 64(10), 1015–1025 (in Russian).

Plyashkevich, A.A., Minyuk, P.S., Subbotnikova, T.V. and Alshevsky, A.V. (2016) Newly formed minerals of the Fe–P–S system in Kolymsky fulgurite. Doklady Earth Sciences, 467(2), 380-383.

Savina, E.A., Peretyazhko, I.S., Khromova, E.A. and Glushkova, V.E. (2020) Melted rocks (clinkers and paralavas) of Khamaryn-Khural-Khiid combustion metamorphic complex in Eastern Mongolia: mineralogy, geochemistry and genesis. Petrology, 28(5), 431–457.

Seryotkin, Y.V., Sokol, E.V. and Kokh, S.N. (2012) Natural pseudowollastonite: Crystal structure, associated minerals, and geological context. Lithos, 134-135, 75–90.

Shahar, Y., Yaacov, N. and Yair, S. (1989) Two close associations: Si-P-Fe and Si-P-C in the Upper Campanian and Lower Maastrichtian sediments of the Negev, Israel. Sciences Géologiques bulletins, 42(3), 155-171.

Sheldrick, G.M. (2015) Crystal structure refinement with SHELXL. Acta Crystallographica Section C, 71, 3-8.

Sokol, E.V., Novikov, I.S., Vapnik Ye. and Sharygin, V.V. (2007) Gas fire from mud volcanoes as a trigger for the appearance of high-temperature pyrometamorphic rocks of the Hatrurim Formation (Dead Sea area). Doklady Earth Sciences, 413, 474–480.

Sokol, E., Novikov, I., Zateeva, S., Vapnik, Ye., Shagam, R. and Kozmenko O. (2010) Combustion metamorphism in the Nabi Musa dome: new implications for a mud volcanic origin of the Mottled Zone, Dead Sea area. Basin Research, 22, 414–438.

Sokol, E.V., Kozmenko, O.A., Kokh, S.N. and Vapnik Ye. (2012) Gas reservoirs in the Dead Sea area: evidence from chemistry of combustion metamorphic rocks in Nabi Musa fossil mud volcano. Russian Geology and Geophysics, 53, 745–762.

Swam, V. and Dubrovinsky, L.S. (1997) Thermodynamic data for the phases in the $CaSiO_3$ system. Geochimica et Cosmochimica Acta, 61(6), 1181-1191.

Vapnik, Y., Sharygin, V.V., Sokol, E.V. and Shagam, R. (2007) Paralavas in a combustion metamorphic complex: Hatrurim Basin, Israel. Reviews in Engineering Geology, 18, 1–21.

Yang, J.S., Bai, W.J., Rong, H., Zhang, Z.M., Xu, Z.Q., Fang, Q.S., Yang, B.G., Li, T.F., Ren, Y.F., Chen, S.Y., Hu, J.-Z., Su, J.F. and Mao, H.K. (2005) Discovery of Fe_2P alloy in garnet peridotite from the Chinese continental scientific drilling project (CCSD) main hole. Acta Petrolei Sinica, 21, 271–276.

Zolensky, M., Gounelle, M., Mikouchi, T., Ohsumi, K., Le, L., Hagiya, K. and Tachikawa, O. (2008) Andreyivanovite: A second new phosphide from the Kaidun meteorite. American Mineralogist, 93, 1295–1299.

538 **Figure captions**

539 Figure 1. (A) Brecciated rock (I) surrounded by layered low-temperature calcite-hydrogrossular
540 rocks (II); frame shows a fragment magnified in Fig. 1B; (B) Primary breccia of altered country
541 rocks cemented by gehlenite paralava were disintegrated and presented by fragments of different
542 sizes; (C) Large breccia fragment, hydrogrossular rock of pink and grey color in grey amygdaloid
543 gehlenite paralava; (D) Rounded aggregates of the Fe-P(±C) mineral system on the contact of
544 gehlenite paralava and pink hydrogrossular rock. In inset – BSE image of the biggest aggregate
545 showing zonal structure: core – barringerite (Bgr), intermediate zone – schreibersite (Srb), rim –
546 schreibersite-iron (Fe) eutectic.

547 Figure 2. (A) Rounded phosphide aggregates on the boundary of paralava and hydrogrossular
548 rock. The near-contact part of gehlenite paralava is enriched in pseudowollastonite and small
549 xenomorphic inclusions of minerals of the Fe-P(±C) system and pyrrhotite. Frame shows a
550 fragment magnified in Fig. 2B. BSE image. (B) Mineral aggregate of the Fe-P(±C) system at the
551 centrum contains barringerite, and at the rim - Srb-Fe(±Fe_3C) eutectic. Iron is intensively
552 replaced by secondary oxides and phosphates (black spots). BSE images, high contrast. (C,D)
553 Xenomorphic mineral aggregate of the Fe-P(±C) system with fragments presented by Srb-Fe
554 eutectic with different Srb (dark-grey)/Fe ratio. C – BSE, D – reflected light, contrast image. (E)
555 Gehlenite-flamite paralava, BSE. (D) Porous hydrogrossular-tacharanite rock with barringerite
556 relics, BSE. Gh =gehlenie, Flm = flamite, Po =pyrrhotite, Wus =wustite, Fe = native iron, Hgr =
557 hydrogrossular, Scb = schreibersite, Etr = ettringite, Bgr = barringerite, Tch = tacharanite, Cal =
558 calcite, Pwo = pseudowollastonite.

559 Figure 3. (A) Contact of black gehlenite paralava (I) with pink hydrogrossular rock (II), polished
560 plate. Gehlenite paralava contains hollows filled with minerals of the ettringite group and

561 gypsum, calcite and tacharanite. Cr-V-bearing phosphides are in a thin tongue of light paralava
562 (III) in hydrogrossular rock. Red arrow indicates an area magnified in Fig. 3B, yellow arrow – in
563 Fig. 3F; (B) Zonal aggregate with schreibersite and low-chromian barringerite (1 group, Table 1);
564 (C) Xenomorfic grains of allabogdanite (4a group, Table 1) in association with xenomorphic
565 fluorapatite and perovskite grains and orthogonal pseudomorph of hydrogrossular after gehlenite.
566 Hydrogarnet forming a reactive rim on allabogdanite is enriched in Fe and Cr; (D) Xenomorphic
567 grains of andreyivanovite (5b group, Table 1) in tacharanite; (F) Graphite crystal inclusions in
568 phosphide aggregates and osbornite intergrows with phosphides. In the inset, there is the same
569 area in reflected light, copper-golden color of osbornite is a characteristic property. B-E – BSE
570 images. Abg = allabogdanite, Aiv = andreyivanovite, Bgr = barringerite, Cal = calcite, Csp =
571 cuspidine, Fap = fluorapatite, Gr = graphite, Hgr = hydrogarnet, Prv = perovskite, Pwo =
572 pseudowollastonite, Scb = schreibersite, Tch = tacharanite, Obn = osbornite.
573 Figure 4. (A) Tongue of pseudowollastonite paralava (II) in hydrogrossular rock (I) with Cr- and
574 V-bearing phosphides (white). The cross-section of the paralava tongue is perpendicular to its
575 elongation. Fragments magnified in Fig. 4B, C are shown in frames, BSE. (B, C) Unusual forms
576 of Cr-V-bearing phosphides aggregates (2 and 3 groups, Table 1), BSE. Fragment magnified in
577 Fig. 4D is shown in frames. (D) Light-grey Cr-V-bearing phosphides in reflected light. Csp =
578 cuspidine, Hgr = hydrogrossular, Prv = perovskite, Pwo = pseudowollastonite, Tch = tacharanite.
579 Figure 5. Phosphides analyses in Fe_2P-FeCrP-FeVP ternary diagram: I – EDS analyses, II –
580 microprobe analyses of the grain groups (Arabic numerals) used for the structural investigation.
581 Dashed line divides barringerite and allabogdanite fields.
582 Figure 6. Diagram of correlation of ***c*** parameter (black square) of barringerite and ***b*** parameter of
583 allabogdanite (cross) with Cr+V content.

584 Figure 7. Phase transitions trends in diagram barringerite-allabogdanite (according to Litasov et
585 al. 2020, with simplifications): 1 – experiment (Dera et al. 2008); 2 – meteorite, crystallization
586 from melt as a result of impact event (Britvin et al. 2019); 3 – meteorite, barringerite -
587 allabogdanite phase transition (Litasov et al. 2020); 4 –paralava, formation of terrestrial
588 allabogdanite after barringerite as a result of meteorite impact (Britvin et al. 2021); 5 – paralava,
589 barringerite - allabogdanite phase transition.
590
591
592
593
594

This is the peer-reviewed, final accepted version for American Mineralogist, published by the Mineralogical Society of America.
The published version is subject to change. Cite as Authors (Year) Title. American Mineralogist, in press.
DOI: https://doi.org/10.2138/am-2022-8647. http://www.minsocam.org/

Table 1. Chemical composition of Cr-V-bearing phosphides from pseudowollastonite paralava, wt.%

group	1a		1b		2			3		
wt.%	n= 3	s.d.	n= 4	s.d.	n= 8	sd	range	n= 12	s.d.	range
P	22.12	0.10	21.83	0.15	22.06	0.11	21.96-22.30	22.38	0.10	22.19-22.54
Ca	0.13	0.05	0.11	0.04	0.12	0.09	0.04-0.33	0.23	0.04	0.17-0.31
Cu	0.10	0.06	0.13	0.05	0.17	0.04	0.11-0.22	0.11	0.02	0.06-0.15
Ni	0.12	0.02	0.14	0.02	0.06	0.05	0.02-0.17	0.02	0.03	0.00-0.08
Fe	74.88	0.45	74.08	0.33	67.84	0.13	67.55-67.98	62.36	0.29	61.88-62.82
Cr	2.00	0.12	2.22	0.15	7.20	0.13	6.90-7.35	10.10	0.12	9.85-10.31
V	0.70	0.16	1.02	0.17	2.17	0.04	2.11-2.26	4.09	0.10	3.92-4.24
Ti	0.11	0.04	0.08	0.03	0.29	0.07	0.15-0.38	0.28	0.05	0.18-0.37
Total	100.16		99.61		99.90			99.58		
calculated on 3 atoms										
P	1.012		1.005		1.007			1.019		
Ca	0.005		0.004		0.004			0.008		
Cu	0.002		0.003		0.004			0.002		
Ni	0.003		0.003		0.001			0.000		
Fe	1.901		1.892		1.718			1.575		
Cr	0.055		0.061		0.196			0.274		
V	0.019		0.029		0.060			0.113		
Ti	0.003		0.002		0.009			0.008		

Table 1. continuation

group	4a			4b		4c			5a			5b	
wt.%	n= 7	s.d.	range	n= 4	s.d.	n=10	s.d.	range	n=6	s.d.	range	n=3	s.d.
P	22.53	0.09	22.41-22.65	22.52	0.04	22.45	0.07	22.34-22.56	22.63	0.09	22.51-22.78	22.44	0.03
Ca	0.18	0.07	0.09-0.31	0.28	0.02	0.45	0.15	0.29-0.82	0.33	0.24	0.11-0.80	0.70	0.21
Cu	0.07	0.04	0.03-0.15	0.06	0.02	0.06	0.03	0.01-0.11	0.18	0.09	0.07-0.37	0.09	0.07
Ni	0.07	0.02	0.03-0.10	0.02	0.01	0.02	0.02	0.00-0.07	0.02	0.02	0-0.06	0.05	0.02
Fe	56.70	0.22	56.26-56.97	54.56	0.07	56.43	0.34	55.60-56.81	53.52	1.69	50.15-54.97	48.29	0.96
Cr	14.19	0.11	14.06-14.37	14.56	0.16	12.87	0.25	12.20-13.17	16.80	0.17	16.49-16.99	18.48	0.12
V	5.25	0.09	5.13-5.36	6.52	0.08	6.63	0.24	6.35-7.14	5.68	1.54	4.47-8.63	8.36	0.90
Ti	0.47	0.04	0.40-0.51	0.66	0.02	0.56	0.05	0.42-0.60	0.42	0.11	0.26-0.57	0.46	0.08
Total	99.45			99.18		99.47			99.58			98.87	
Calculated on 3 atoms													
P	1.022			1.022		1.017			1.022			1.017	
Ca	0.006			0.010		0.016			0.012			0.025	
Cu	0.002			0.001		0.001			0.004			0.002	
Ni	0.002			0.000		0.000			0.000			0.001	
Fe	1.426			1.373		1.418			1.341			1.213	
Cr	0.383			0.394		0.347			0.452			0.499	
V	0.145			0.180		0.183			0.156			0.230	
Ti	0.014			0.019		0.016			0.012			0.013	

This is the peer-reviewed, final accepted version for American Mineralogist, published by the Mineralogical Society of America.
The published version is subject to change. Cite as Authors (Year) Title. American Mineralogist, in press.
DOI: https://doi.org/10.2138/am-2022-8647. http://www.minsocam.org/

Table 2. Unit cell parameters, crystal chemical formulas and electron density at Fe2 site of Cr-V-bearing phosphides of the assigned groups

	Structural parameters			*Chemical data*	*Fe2 site*	
	a	*b*	*c*		SCXRD	EMPA
		P-62m		simplified formula	Sof/e-	e-
1b/18*	5.8565(3)	5.8565(3)	3.4712(2)	$Fe_{1.89}Cr_{0.06}V_{0.03}P_{1.01}$	0.986(5)/25.64	25.79
1a/23	5.8588(3)	5.8588(3)	3.4673(2)	$Fe_{1.90}Cr_{0.05}V_{0.02}P_{1.01}$	0.987(5)/25.66	25.84
2/3	5.8414(3)	5.8414(3)	3.4922(2)	$Fe_{1.72}Cr_{0.20}V_{0.06}Ti_{0.01}P_{1.01}$	0.964(7)/25.06	25.38
		Pnma				
2/7	5.8003(3)	3.5665(3)	6.6405(4)	$Fe_{1.72}Cr_{0.20}V_{0.06}Ti_{0.01}P_{1.01}$	0.968(3)/25.17	25.38
2/9	5.8020(2)	3.5664(1)	6.6448(3)	$Fe_{1.72}Cr_{0.20}V_{0.06}Ti_{0.01}P_{1.01}$	0.971(5)/25.25	25.38
3/61	5.8165(4)	3.5664(2)	6.6531(4)	$Fe_{1.57}Cr_{0.27}V_{0.11}Ti_{0.01}Ca_{0.01}P_{1.02}$	0.956(5)/24.85	25.09
4a/68	5.8269(6)	3.5624(4)	6.6599(8)	$Fe_{1.42}Cr_{0.35}V_{0.18}Ti_{0.02}Ca_{0.02}P_{1.02}$	0.933(3)/24.26	24.68
4b/1	5.8269(4)	3.5689(3)	6.6627(5)	$Fe_{1.43}Cr_{0.38}V_{0.14}Ti_{0.01}Ca_{0.01}P_{1.02}$	0.950(8)/24.70	24.78
4c/62	5.8307(3)	3.5645(2)	6.6617(4)	$Fe_{1.37}Cr_{0.39}V_{0.18}Ti_{0.02}Ca_{0.01}P_{1.02}$	0.925(2)/24.05	24.60
5a/64	5.8231(3)	3.5666(2)	6.6564(3)	$Fe_{1.34}Cr_{0.45}V_{0.16}Ti_{0.01}Ca_{0.01}P_{1.02}$	0.933(4)/24.26	24.58

*- group number/grain number, Sof – Fe occupancy, e- - electron density, SCXRD – structural data, EMPA – data of electron microprobe analysis

This is the peer-reviewed, final accepted version for American Mineralogist, published by the Mineralogical Society of America.
The published version is subject to change. Cite as Authors (Year) Title. American Mineralogist, in press.
DOI: https://doi.org/10.2138/am-2022-8647. http://www.minsocam.org/

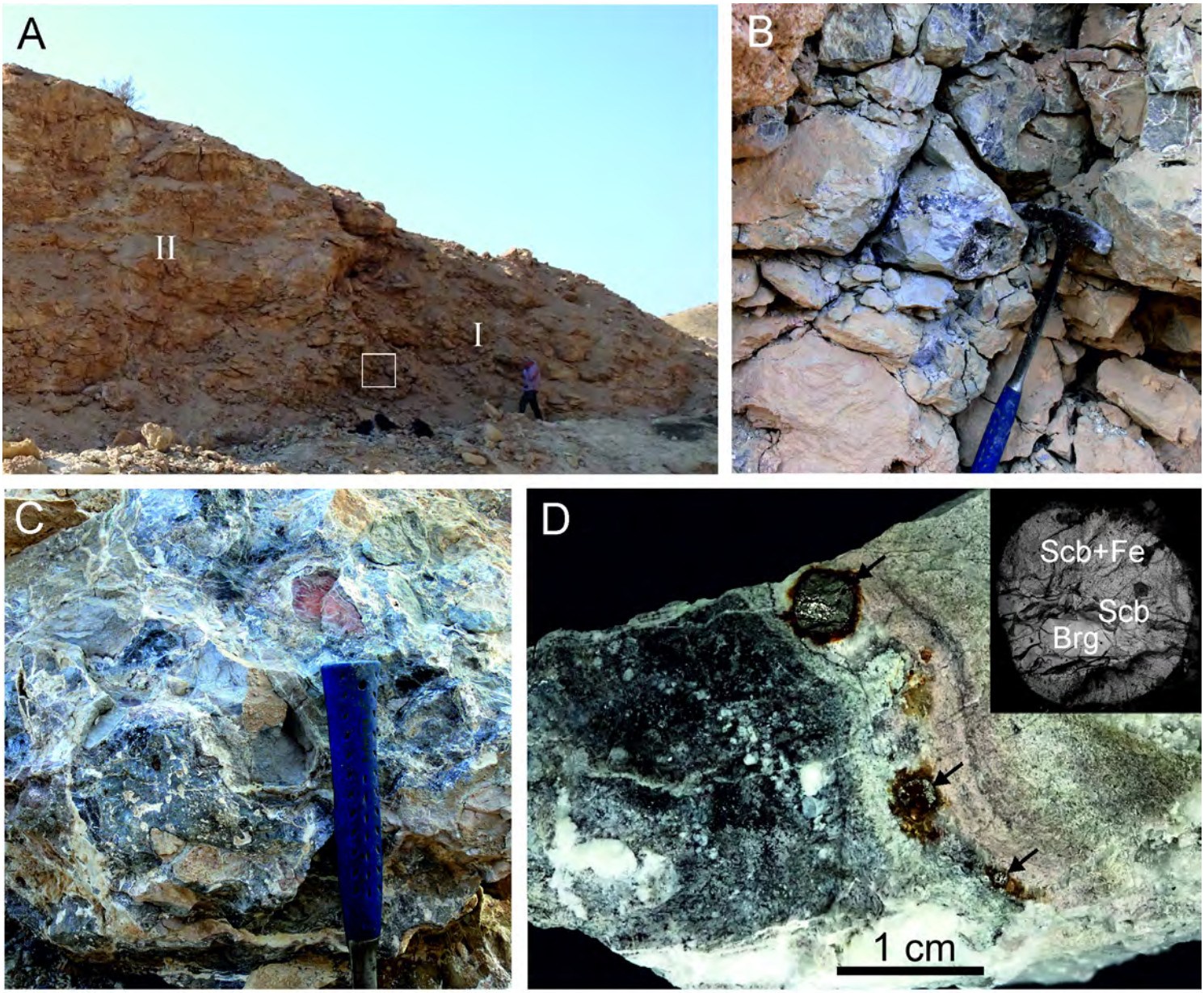

Figure 1

This is the peer-reviewed, final accepted version for American Mineralogist, published by the Mineralogical Society of America.
The published version is subject to change. Cite as Authors (Year) Title. American Mineralogist, in press.
DOI: https://doi.org/10.2138/am-2022-8647. http://www.minsocam.org/

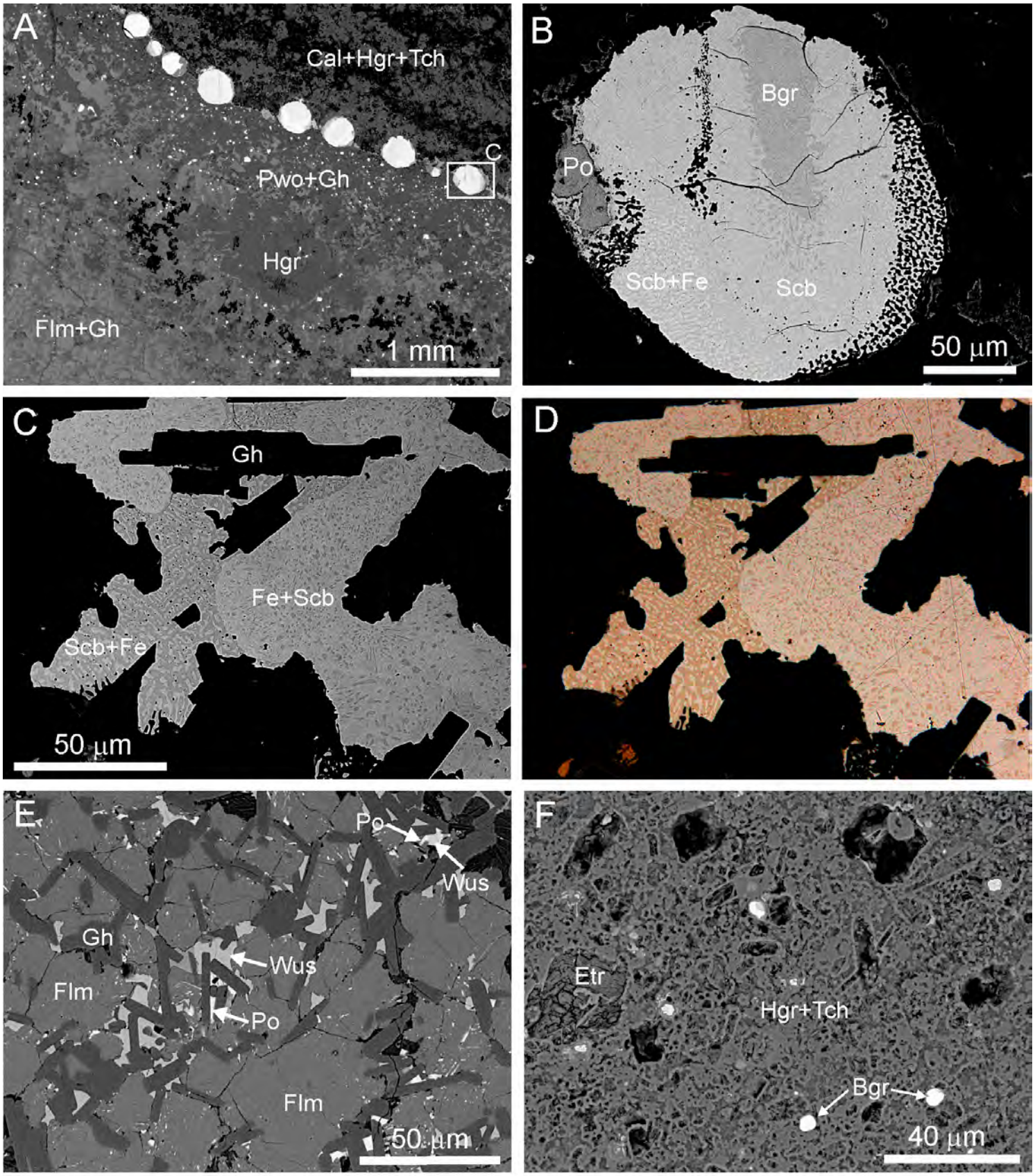

Figure 2

This is the peer-reviewed, final accepted version for American Mineralogist, published by the Mineralogical Society of America.
The published version is subject to change. Cite as Authors (Year) Title. American Mineralogist, in press.
DOI: https://doi.org/10.2138/am-2022-8647. http://www.minsocam.org/

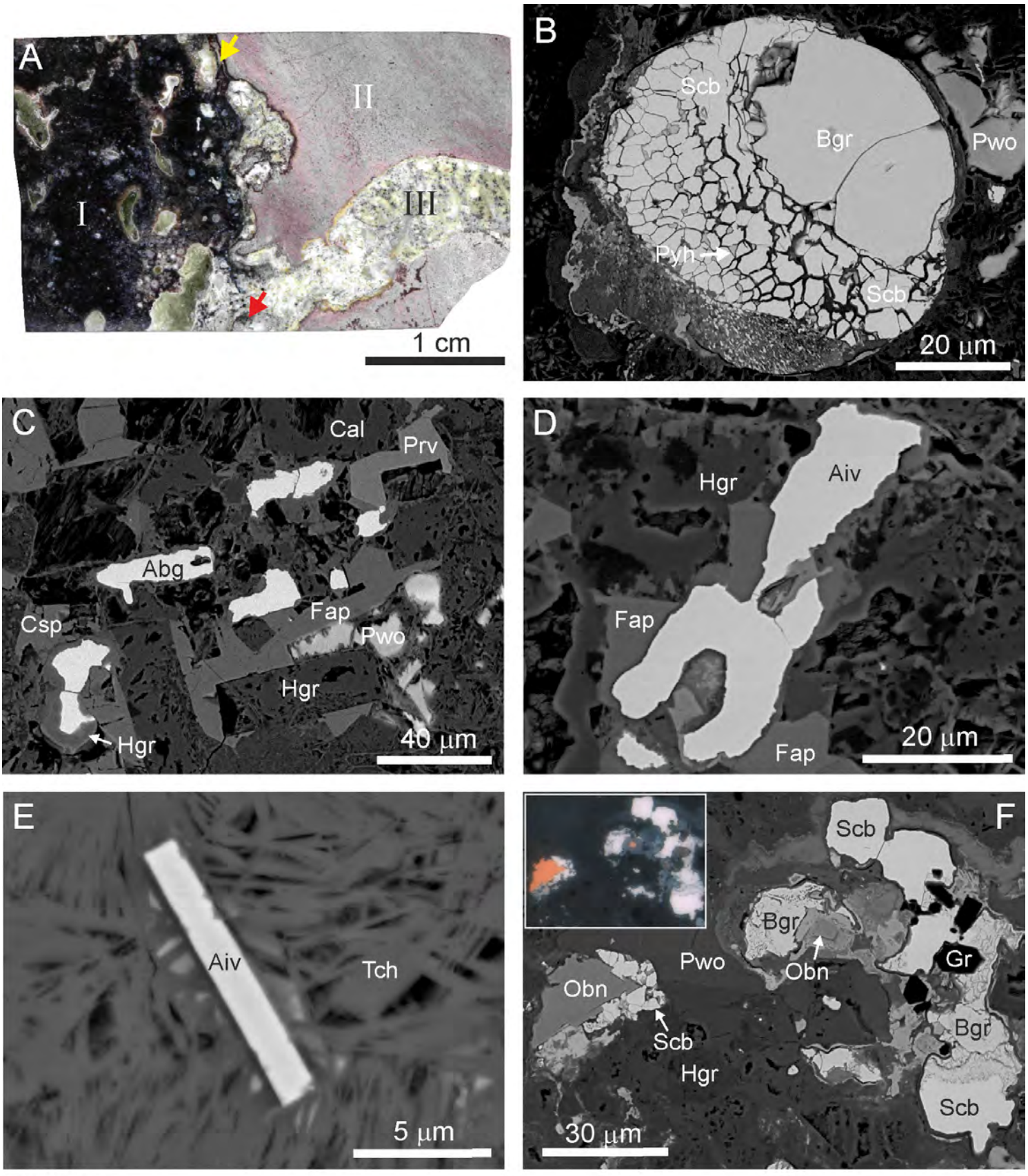

Figure 3

This is the peer-reviewed, final accepted version for American Mineralogist, published by the Mineralogical Society of America.
The published version is subject to change. Cite as Authors (Year) Title. American Mineralogist, in press.
DOI: https://doi.org/10.2138/am-2022-8647. http://www.minsocam.org/

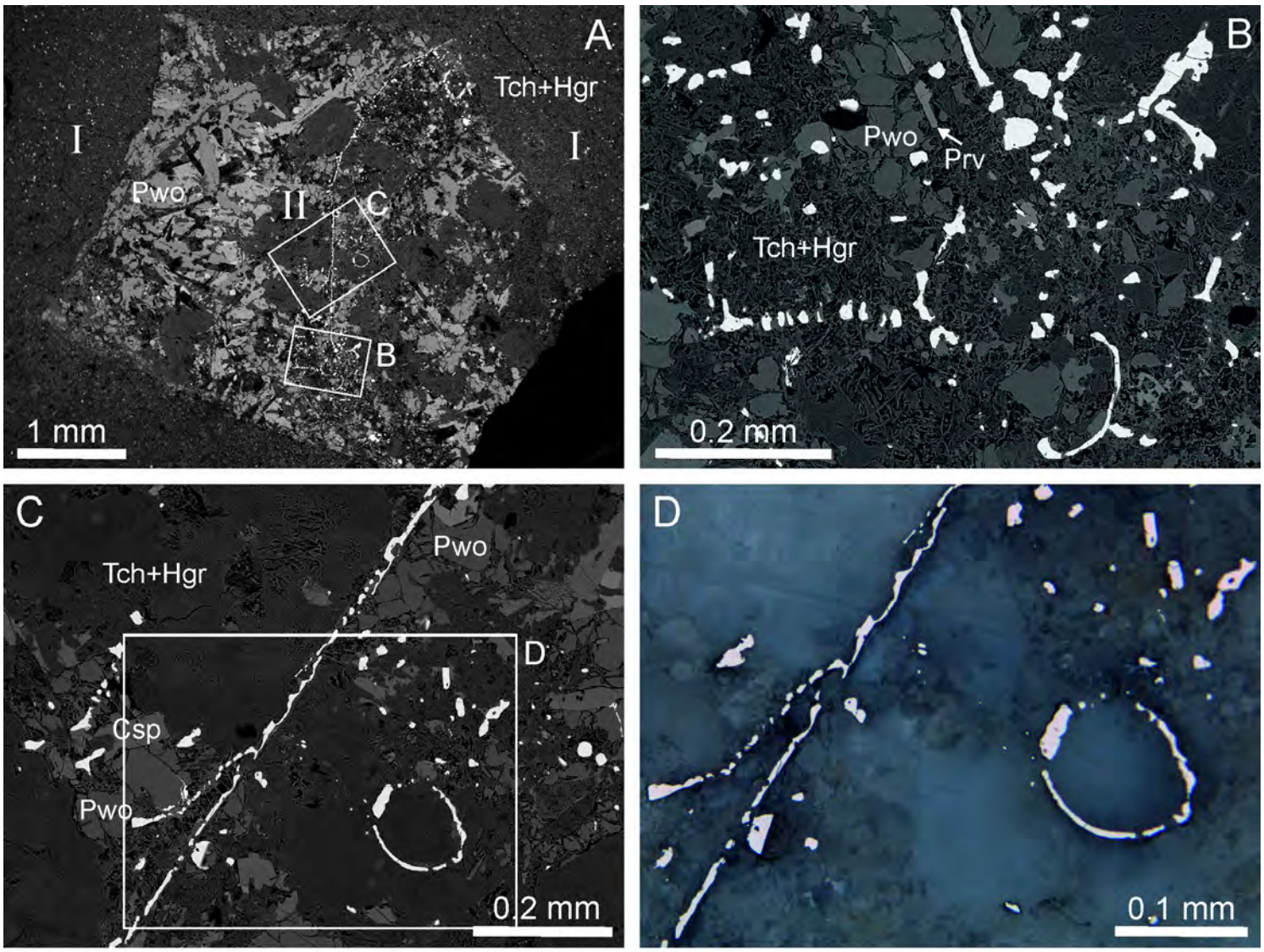

Figure 4

This is the peer-reviewed, final accepted version for American Mineralogist, published by the Mineralogical Society of America.
The published version is subject to change. Cite as Authors (Year) Title. American Mineralogist, in press.
DOI: https://doi.org/10.2138/am-2022-8647. http://www.minsocam.org/

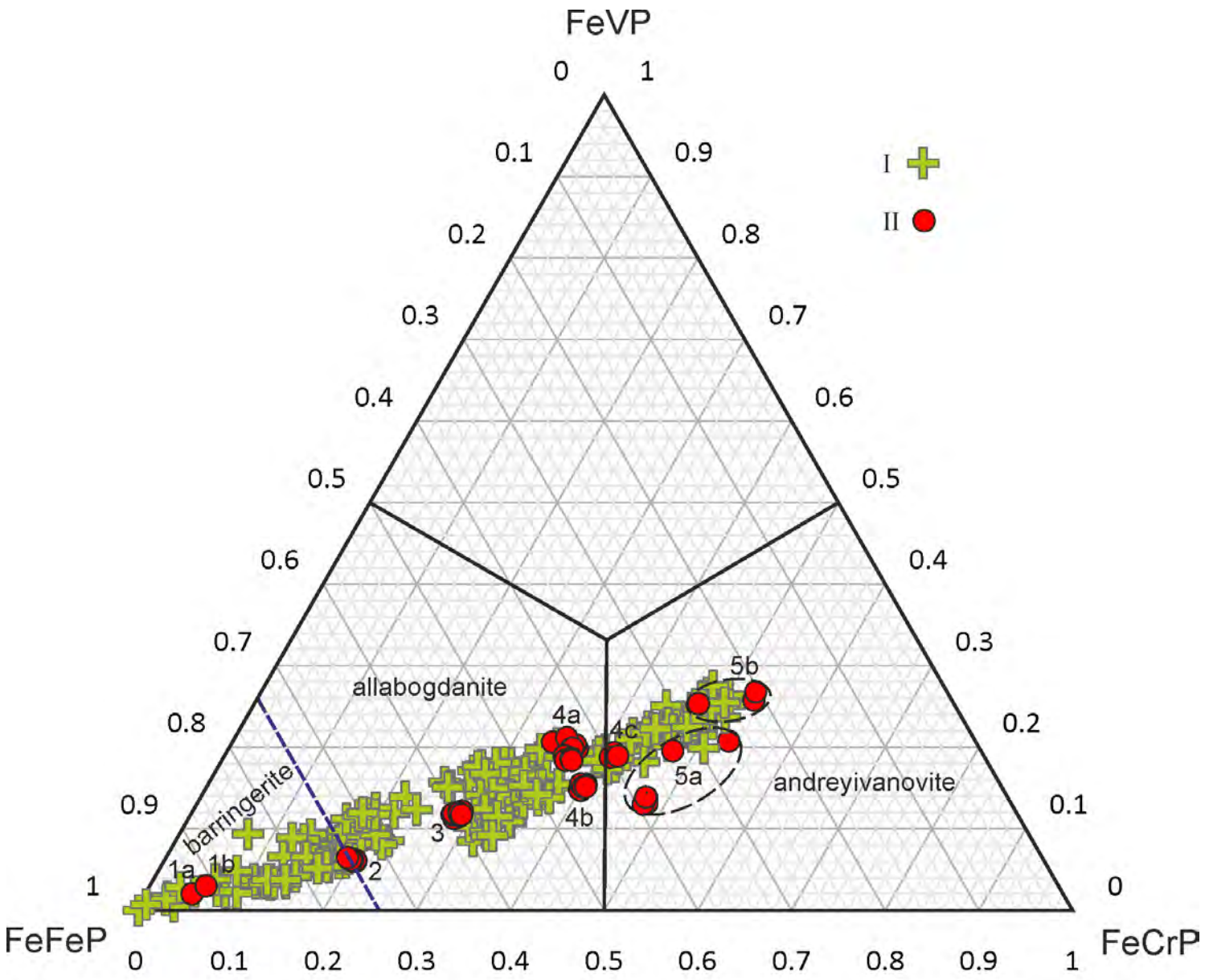

Figure 5

This is the peer-reviewed, final accepted version for American Mineralogist, published by the Mineralogical Society of America.
The published version is subject to change. Cite as Authors (Year) Title. American Mineralogist, in press.
DOI: https://doi.org/10.2138/am-2022-8647. http://www.minsocam.org/

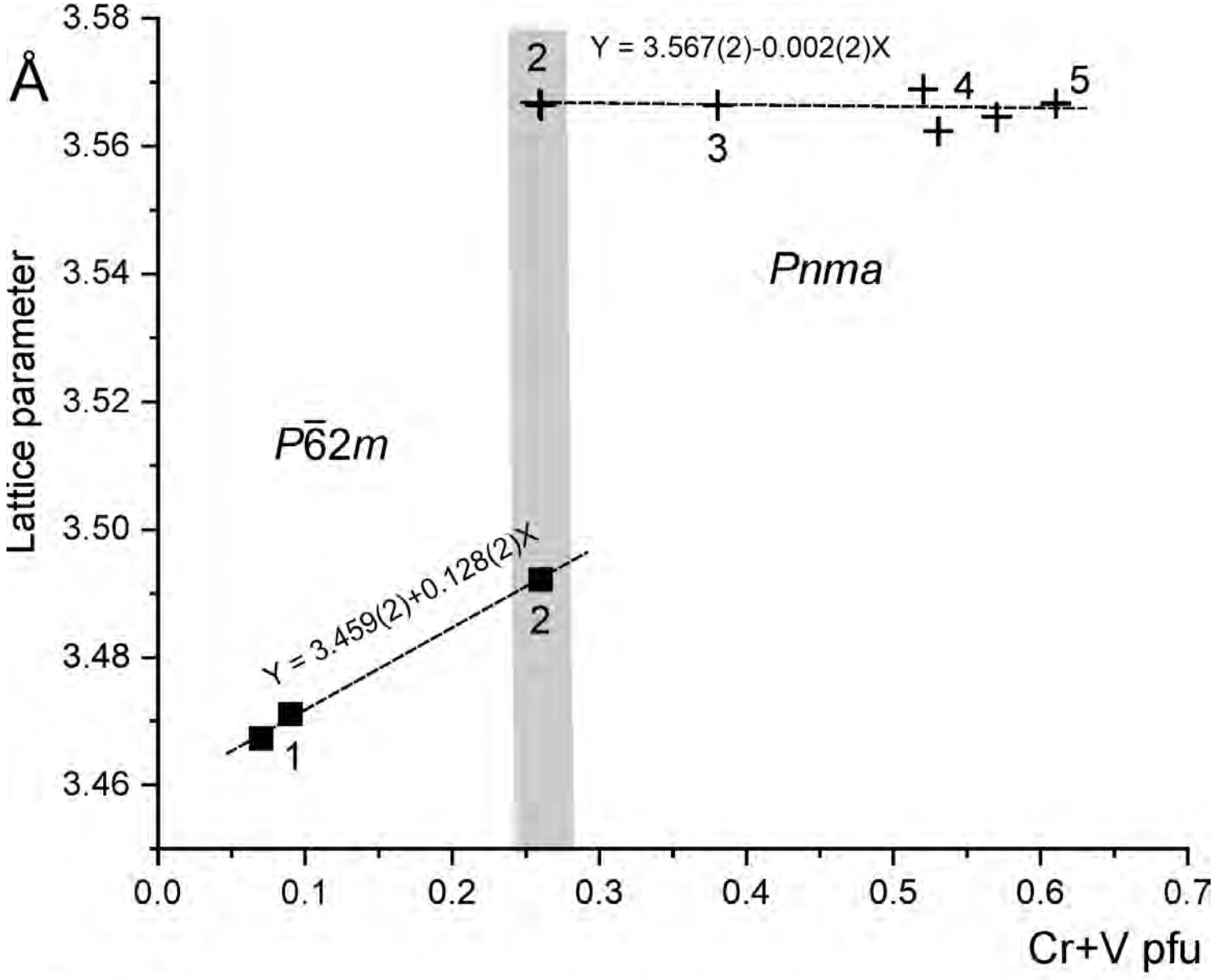

Figure 6

This is the peer-reviewed, final accepted version for American Mineralogist, published by the Mineralogical Society of America.
The published version is subject to change. Cite as Authors (Year) Title. American Mineralogist, in press.
DOI: https://doi.org/10.2138/am-2022-8647. http://www.minsocam.org/

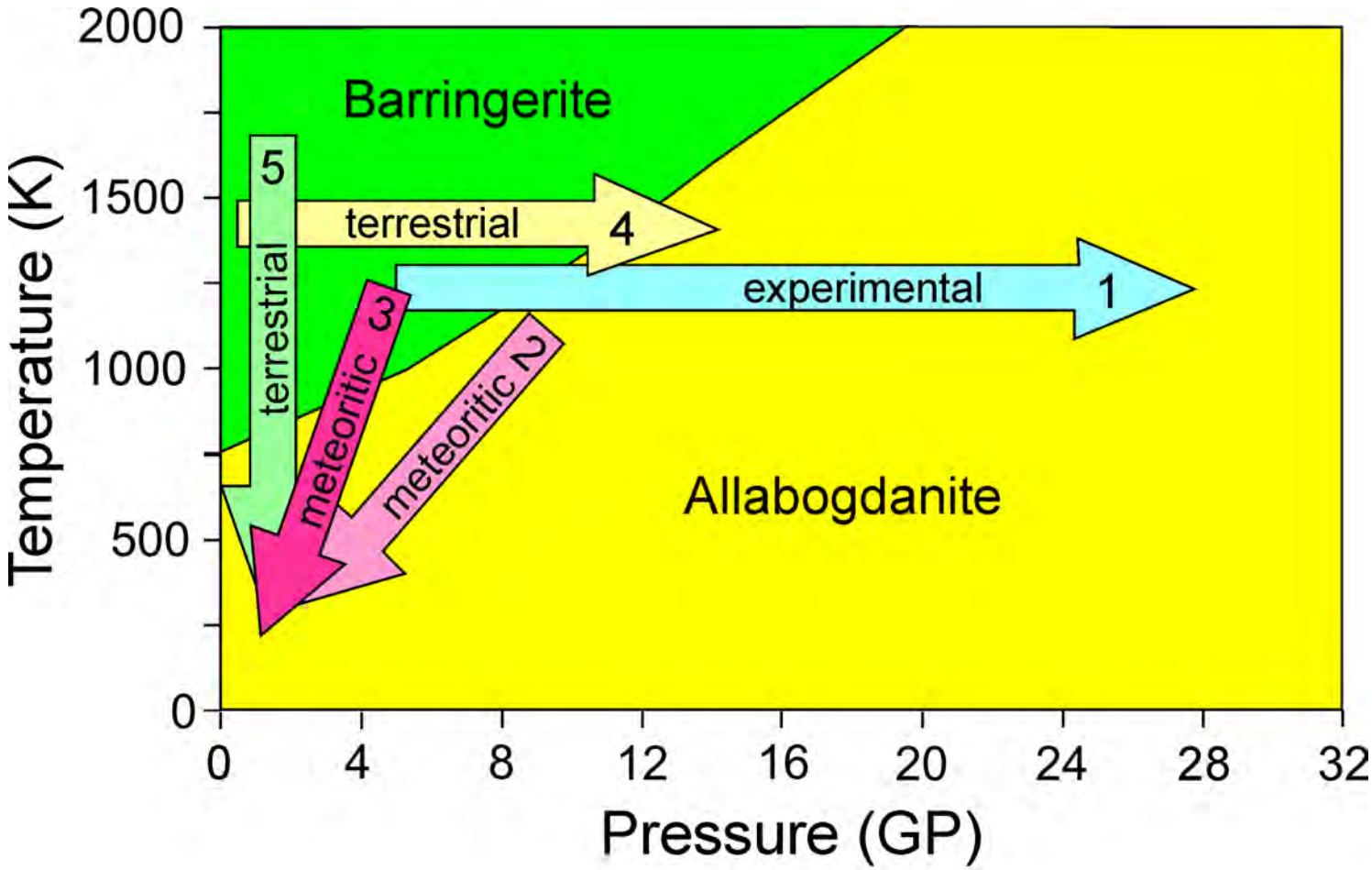

Figure 7